Relativistic effects on the Compton profile of polycrystalline gold

1993 J. Phys.: Condens. Matter 5 977

(http://iopscience.iop.org/0953-8984/5/7/025)

J. Phys.: Condens. Matter 5 (1993) 977–990. Printed in the UK

Relativistic effects on the Compton profile of polycrystalline gold

Helmut Reinisch and Helmut Bross

Sektion Physik der Universität München, Theresienstrasse 37, D-8000 München 2, Federal Republic of Germany

Received 22 May 1992, in final form 9 November 1992

Abstract. The spherically averaged Compton profile (CP) for gold is calculated on the basis of the relativistic density-functional theory in the local-density approximation (LDA) with a warped muffin-tin potential. In the all-electron self-consistent procedure, the core levels are calculated by means of the Dirac operator while the valence levels are determined by a relativistic generalization of the modified augmented plane-wave (MAPW) method using the reduced 2×2 matrix Hamiltonian according to Foldy and Wouthuysen. The CPs of the core electrons are found to be in surprisingly good agreement with the orbital CPs of the relativistic Hartree–Fock calculation for atomic gold by Biggs *et al.* The relativistic corrections on the valence CP due to mass–velocity and the Darwin term are investigated separately and comparisons with non-relativistic calculations are made.

1. Introduction

For 30 years the density-functional theory [1] has been used extensively for the investigation of crystal ground-state properties. Within this theory, it is possible to determine the electron charge and spin density, as well as the total binding energy and related quantities such as the magnetic susceptibility, equilibrium lattice constant and bulk modulus [2]. A set of single-particle equations with an effective potential for auxiliary particles must be solved self-consistently [3]. The only quantity that needs to be approximated is the exchange–correlation energy functional $E_{xc}[n]$, and in most cases the simplest approximation for $E_{xc}[n]$, the local-density approximation (LDA), is used. In this one-particle scheme the calculation of further properties than those mentioned above is established by means of the wavefunctions that are solutions of the single-particle equations. Though this procedure is not rigorously confirmed, it provides in most cases the best available description of the ground state and the excited states of transition metals. In this framework the examination of the electron momentum density, the Compton profile (CP), and the influence of relativistic corrections on it is the main purpose of the present paper. Here the relativistic extension of the density-functional theory [4, 5] is applied, and exchange and correlation are treated in terms of the Gunnarsson–Lundqvist approach [6] with the relativistic correction according to MacDonald and Vosko [7]. Alternatively, the momentum analogue of the spatial Hohenberg–Kohn theorem [8] would permit direct calculation of the electron momentum-space density without loss of rigour, but until now only non-relativistic considerations and crude approximations for the momentum-space energy functionals have been available [9].

0953-8984/93/070977+14$07.50

The spherical mean value $J(q)$ of the CP is related to the spherical mean value $n(p)$ of the electron momentum density by [10]

$$J(q) = 2\pi \int_q^\infty \mathrm{d}p\, pn(p). \tag{1}$$

Within the so-called impulse approximation [11] $J(q)$ is proportional to the differential cross section [10] and therefore directly measurable by γ-ray scattering experiments on polycrystalline matter. This concept holds even in a relativistic context near the Compton line for electrons with small binding energies, i.e. valence electrons [12]. That means that the total differential cross section is accurate enough in this area, as the contribution of the valence electrons dominates.

Compton scattering studies on transition metals involving the use of polycrystalline samples aim at the determination of absolute CPs. More recent measurements use single crystals to obtain their directional dependence. After convoluting the theoretical absolute profile with the residual instrument function, the agreement with experiment was found to be good in many cases [13–20], when the renormalized free atom (RFA) model [21] with a suitably chosen electronic configuration for the outer electrons was used. The agreement turns out to be worse in the case of more accurate electron band-structure calculations like the augmented plane-wave (APW)—or linear combination of atomic orbitals (LCAO)—method, when no fitting parameter is used. Independently of the quality of the particular band model, theoretical directional difference profiles are approximately a factor of 2 larger than the measured ones [22], which has been interpreted as a drawback of the LDA [23].

Only a few relativistic treatments have been carried out so far. Apart from spin-polarized calculations, there is only one self-consistent band-structure calculation of valence CPs of crystals, which however takes into account only scalar-relativistic effects. This calculation by Papanicolaou *et al* [24] on tantalum and tungsten makes use of the method of Koelling and Harmon [25] to include Darwin and mass–velocity relativistic corrections in an overall manner, but neglects the spin–orbit coupling. The discrepancy between this calculation and measurements on tungsten by Mittal *et al* [15] turns out to be 4% for the absolute profile $J(0)$. It was supposed that this difference originates from the neglect of spin–orbit coupling. But the present investigation shows that this effect contributes only 0.1% in the case of gold, which has an even higher atomic number.

With increasing nuclear charge, competitive processes like photoabsorption and Rayleigh scattering make the evaluation of CPs from experimental data of heavy elements difficult. That is why no γ-ray valence CP data of gold crystals have been reported until now. The present work aims to stimulate such measurements, as it forms a basis for the analysis of the experimental data. The only experimental investigation of the valence CP of gold [26] makes use of proton–electron scattering yielding the so-called ion CPs which resemble in many details conventional γ-ray CPs. As physically interesting effects change CP lineshapes only by small amounts, this paper discusses separately the influence of the various relativistic corrections on the valence CP and shows their relevance. The contribution to the CP due to the core electrons is determined within the density-functional theory using a very effective integration method and is compared with the orbital CPs of the relativistic Hartree–Fock calculation for atomic gold by Biggs *et al* [27].

2. Band structure

For simplification, the one-particle equation is solved within the warped muffin-tin shape approximation of the effective potential $V_{\text{eff}}(r)$. All states spatially localized inside the Slater sphere with $|r|$-dependent potential $V_{\text{eff}}(r)$ are found by solving the four-component Dirac equation. These correspond to the 46 electrons that occupy the levels 1s–4d.

Different band-structure methods have been developed in the past (see, e.g., [28]) for the valence electrons. Their relativistic generalization is based either on the four-component Dirac equation or on a two-component formalism. An advantage of the latter is that it offers the possibility for a 'quasi-relativistic' approach where spin–orbit interaction is neglected. Its use in self-consistent procedures requires the norm conservation of the two-component wavefunctions ψ for the calculation of the electron charge density. This requirement is fulfilled by decoupling the large and small components of the Dirac equation via successive application of unitary Foldy–Wouthuysen transformations [29], yielding a quasi-relativistic two-component Pauli-type equation. Decoupling up to second order in the fine-stucture constant α results in corrections to the kinetic energy (of mass–velocity type) $\mathcal{H}_{\text{mv}}$ and to the potential (Darwin term) $\mathcal{H}_{\text{d}}$ and introduces spin–orbit coupling $\mathcal{H}_{\text{so}}$ into the Schrödinger equation. The resulting Hamiltonian has successfully been used in atomic [30] and band-structure [31] calculations.

Difficulties might arise when determining the relativistic corrections of the variational expression. The effective potential is not continuous on the surface of the Slater sphere owing to the warped muffin-tin approximation. Therefore the expectation values are unambiguously determined only if ψ fulfils the minimal condition to be continuously differentiable in the whole Wigner–Seitz cell (WSC), which moreover ensures the physical condition of current conservation. Marcus [32] gives various arguments as to how to interpret these expectation values for trial functions violating the minimal condition. But different parameters must be chosen in an appropriate but not unambiguous way.

The modified augmented plane-wave method (MAPW) is well suited for the problem under discussion because the MAPW wavefunction and its first derivative are exactly continuous on the surface of the Slater sphere and the wavefunctions of the valence electrons are orthogonal to the wavefunctions of the core electrons [33–37]. A four-component relativistic generalization of the MAPW method was done by Hofmann and Bross [38] and applied by Schiekel [39]. For a two-component generalization used here, one has to replace the real scalar expansion coefficients by complex spinors. Results for the matrix elements of the Hamiltonian with the MAPW *ansatz* functions can be found in [40]. Details about the self-consistent procedure and how the self-consistent potential may be obtained from the MAPW formalism are described elsewhere [41].

3. Compton profile

All one-particle states in the crystal lattice have the Bloch form $\psi_{nk}(r) = \exp(ik \cdot r)u_{nk}(r)$, where $u_{nk}(r)$ has the periodicity of the crystal lattice. Their Fourier transforms are given by

$$\psi_{nk}(p) = \frac{1}{V_{bz}^{1/2}} \int_{\mathcal{V}} d^3r \, \frac{\exp(-ip \cdot r)}{\mathcal{V}^{1/2}} \psi_{nk}(r). \tag{2}$$

Here n is the band index in the case of valence electrons or contains the quantum numbers $\{n, j, l, m\}$ (with usual meaning) in the case of atomic states; k is the reduced wavevector, and V_{bz} and $\mathcal{V}$ denote the volumes of the first Brillouin zone and the bulk, respectively. When the initial and final spin states are not observed in scattering experiments, the electron momentum density is the trace with respect to the spin:

$$\begin{aligned} n_{nk}(p) &= \psi_{nk}^{\dagger}(p)\psi_{nk}(p) \\ n(p) &= \frac{1}{V_{bz}} \sum_{n} \int_{V_{bz}} d^3k \, \Theta(E_f - E_{nk}) n_{nk}(p) \end{aligned} \tag{3}$$

where the Θ-function admits only occupied electron states with energy levels E_{nk} less than the Fermi energy E_f.

3.1. Core levels

Evaluating equations (2) and (3) with the solution of the Dirac equation for core electrons yields for shells fully occupied with respect to the magnetic quantum number $(-j \leqslant m \leqslant j)$ the following electron momentum density:

$$\begin{aligned} n_{njl}(p) = \frac{1}{2\pi^2} \Bigg[&\left(\int_0^{\infty} dr \, r^{\rho+1} \mathcal{J}_l(pr) g_{njl}(r) \right)^2 \\ &+ \alpha^2 \left(\int_0^{\infty} dr \, r^{\rho+1} \mathcal{J}_{l'}(pr) f_{njl}(r) \right)^2 \Bigg]. \end{aligned} \tag{4}$$

Here $r^{\rho-1}g(r)$ and $r^{\rho-1}f(r)$ are radial functions of the large and small components of the Dirac wavefunction with $\rho = [\kappa^2 - (Z\alpha)^2]^{1/2}$, $l' = l + s$, $j = l + s/2$, $\kappa = -s(j + 1/2)$, $s = \pm 1$ and $Z = 79$ is the atomic number of gold. The normalization conditions of the momentum density and of the CP

$$4\pi \int_0^{\infty} dp \, p^2 n_{njl}(p) = \int_{-\infty}^{\infty} dq \, J_{njl}(q) = 1 \tag{5}$$

can be used as a check for the accuracy of the calculations. Owing to the localization of the functions g and f the integral appearing in equation (1) has to be extended to high momenta. This causes two difficulties. First, in the high-momentum region the integrands in equation (4) show a highly oscillatory behaviour because of the Bessel functions; and secondly, one is compelled to cut off the integration p-mesh at a certain maximum value p_{∞}. The first difficulty is avoided in the following way: The effective charge $Z_{eff}(r) = rV_{eff}(r)$ given on a mesh r_i is interpolated by a cubic spline function, which is continuous up to the second derivative at each point and is, of course, analytical in each interval $r \in [r_i, r_{i+1}]$. Therefore, the Dirac equation is solved by virtue of the series

$$h(r) = \sum_{\nu=0}^{\infty} h_{\nu}(r - r_i)^{\nu} \qquad r \in [r_i, r_{i+1}]$$

for each interval, where h stands for the functions $g(r)$, $f(r)$ and $\mathcal{J}_l(pr)/(pr)^l$. These functions are chosen such that $h_0 \neq 0$, where the last function belongs to the special values $V_{\text{eff}} = 0$, $\alpha = 0$ and $E = p^2$. The expansion coefficients h_ν obey recursion relations, from which they are easily obtained by consideration of the boundary conditions at each knot of the r-mesh. Applying the same technique, the integrals of equation (4)

$$I = p^l \int_0^{r_\infty} \mathrm{d}r\, r^{l+\rho+1} t(r)$$

where $t(r)$ is the product of the function $\mathcal{J}_l(pr)/(pr)^l$ with $g(r)$ and $f(r)$ respectively, are found by solving the corresponding inhomogeneous differential equation:

$$(l+\rho+2)\mathcal{I}(r)+r\mathcal{I}'(r) = t(r) \qquad \mathcal{I}(0) = \frac{t(0)}{l+\rho+2} \qquad I = p^l (r_\infty)^{l+\rho+2} \mathcal{I}(r_\infty).$$

Here r_∞ is the cut-off value of the r-mesh, for which the conditions $g(r_\infty) = 0$ and $f(r_\infty) = 0$ are fulfilled with sufficient numerical accuracy. As long as the potential is defined by the cubic spline function, the described method is free of systematic errors. Almost all one-dimensional problems appearing in the present work like one-dimensional integrals and ordinary differential equations are treated by analogous procedures. Due to cancellation of digits, loss of accuracy occurs only for p-values higher than 500 au when the machine precision comes to 14 decimal digits. Extending the p-integration up to this value produces an error of less than 0.025% even for the most critical case, the 1s electron with the broadest CP. This estimation results by comparing the numerical value of the CP in the long-wave limit $J_{1s}^c(q = 0)$ for the 1s electron in the Coulomb potential with its analytical value (see appendix):

$$J_{1s}^c(0) = \frac{(\rho+1)(2\rho+1)}{8\pi^{1/2}\rho Z} \frac{\Gamma(\rho+1)}{\Gamma(\rho+3/2)} [2\rho - 2 + \psi(\rho+3/2) - \psi(1/2)]. \tag{6}$$

In equation (6), $\Gamma(z)$ and $\psi(z)$ denote the usual gamma and psi functions, respectively. $J_{1s}^c(0) = 0.0091642\,9$ au results for $\alpha = 1/137.035\,968$ [42].

3.2. Valence levels

The Fourier transform $u_{nk}(K)$ of the lattice-periodic part $u_{nk}(r)$ of the MAPW *ansatz* function can be expressed explicitly by the MAPW *ansatz* spinors A and v in the form [43]:

$$\begin{aligned} u_{nk}(K) = V_{\text{wsc}}^{1/2} v_{nk}(K) + \frac{4\pi}{V_{\text{wsc}}^{1/2}} \sum_{l=0}^{l_{\max}} (2l+1) \sum_{\nu=1}^{2l+1} \eta_{l\nu} \mathcal{Y}_{l\nu}(k+K) \\ \times \left(\sum_E A_{nk,El\nu} \int_0^{r_{\text{apw}}} \mathrm{d}r\, r^2 R_{El}(r) \mathcal{J}_l(|k+K|r) \right. \\ \left. - \sum_{K'} v_{nk}(K') \mathcal{Y}_{l\nu}(k+K') \int_0^{r_{\text{apw}}} \mathrm{d}r\, r^2 \mathcal{J}_l(|k+K'|r) \mathcal{J}_l(|k+K|r) \right). \end{aligned} \tag{7}$$

The first integral in equation (7) is evaluated by the method described in the foregoing section. For the second integral—abbreviated by I_l—the following recursion relation is used:

$$I_l = I_{l-2} - (2l-1)r_{\mathrm{apw}}^3 \frac{\mathcal{J}_{l-1}(|k+K'|r_{\mathrm{apw}})}{|k+K'|r_{\mathrm{apw}}} \frac{\mathcal{J}_{l-1}(|k+K|r_{\mathrm{apw}})}{|k+K|r_{\mathrm{apw}}}$$

for $l \geqslant 2$. There exist elementary expressions for I_0 and I_1 with which to start the recursion. The Fourier transform of $\psi_{nk}(r)$ is non-zero only if $p = k + K$. Therefore, using equation (3) one obtains the following sum for $n(p)$:

$$n(p) = \frac{1}{V_{\mathrm{bz}}} \sum_n \Theta(E_{\mathrm{f}} - E_{nk}) u_{nk}^{\dagger}(K) u_{nk}(K) \tag{8}$$

where $p = k + K$ is the decomposition of p into the reduced wavevector k and the reciprocal lattice vector K. At $T = 0$ K the sum is to be extended over the occupied electron states only. The spherical mean value $n(p)$ is determined by a weighted average of $n(p)$ along properly chosen directions [41]. For most applications three different directions are sufficient in the case of cubic structures.

4. Numerical parameters

The lattice constant $a = 7.6813$ was chosen according to Christensen and Seraphin [44]. The radius r_{apw} of the Slater sphere touching the WSC is given by $r_{\mathrm{apw}} = a/\sqrt{8}$ for the FCC lattice. The partition of the interval $[0, r_{\mathrm{apw}}]$ in the form $r_i \propto (i-1)^2$, $i = 1, \ldots, 129$, was taken from Moruzzi *et al* [2] for the representation of the effective potential and the electron charge density. A refinement of the r-mesh such that $r_{i+1} - r_i \simeq 0.1 r_i$, $i = 2, \ldots, 20$, has been proven to be well suited for the integration method used. In the MAPW *ansatz* the maximum value of the angular momentum was $l_{\mathrm{max}} = 3$. Nineteen different *ansatz* energies have been used including the three atom-like levels of the 4f, 5s and 5p electrons. About 60 plane waves, slightly dependent on the k-point, were taken into account according to the condition $(a/2\pi)^2|k+K|^2 \leqslant 15$. The integrations in k-space were carried out with 28 k-points within the irreducible wedge described in detail by Bross [45].

The p-mesh for the integration of the right-hand side of equation (1) was similarly chosen: $p_i \propto (i-1)^2$, $i = 1, \ldots, 301$. In the case of atomic states, the actual upper integration limit $p_\infty = 500(2\pi/a)$ au causes a systematic error of less than 0.025%. The corresponding value for the valence states was chosen to be $60(2\pi/a)$ au. Proceeding in this way the main error results from the spherical averaging process and amounts to about 0.1%.

5. Numerical results and discussion

The present investigations are based on two different potentials. Setting $\alpha = 0$ in all equations yields the self-consistent non-relativistic potential V_{non} with the Hamiltonian $\mathcal{H}_{\mathrm{non}} = -\Delta + V_{\mathrm{non}}$. The second potential V_{rel} is the result of the relativistic self-consistent calculation with all relativistic corrections switched on ($\alpha \neq 0$).

This procedure defines the operator $\mathcal{H}_{rel}$. Note that the proper relativistic effect $\Delta\mathcal{H} = \mathcal{H}_{rel} - \mathcal{H}_{non}$ originates from comparison of the results of these two types of calculation, i.e. from different potentials. For further considerations it is appropriate to split the relativistic correction $\Delta\mathcal{H}$ into parts: $\Delta\mathcal{H} = \Delta\mathcal{H}_{DS} + \Delta\mathcal{H}_V$. Here $\Delta\mathcal{H}_{DS}$ is the difference between the relativistic Hamiltonian and the Schrödinger operator with the potential V_{rel} and $\Delta\mathcal{H}_V = V_{rel} - V_{non}$. For the valence electrons $\mathcal{H}_{DS}$ is well approximated by the sum $\mathcal{H}_d + \mathcal{H}_{mv} + \mathcal{H}_{so}$ (see section 2).

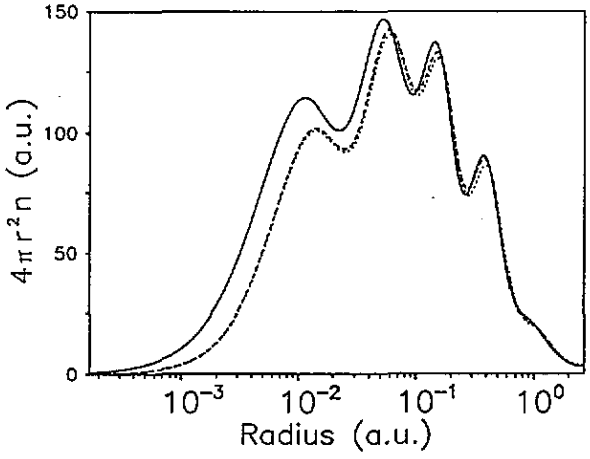

Figure 1. Spherically averaged charge density determined with the operators $-\Delta + V_{rel}$ (·····), $\mathcal{H}_{rel}$ (——) and $\mathcal{H}_{non}$ (– – –), multiplied by $4\pi r^2$.

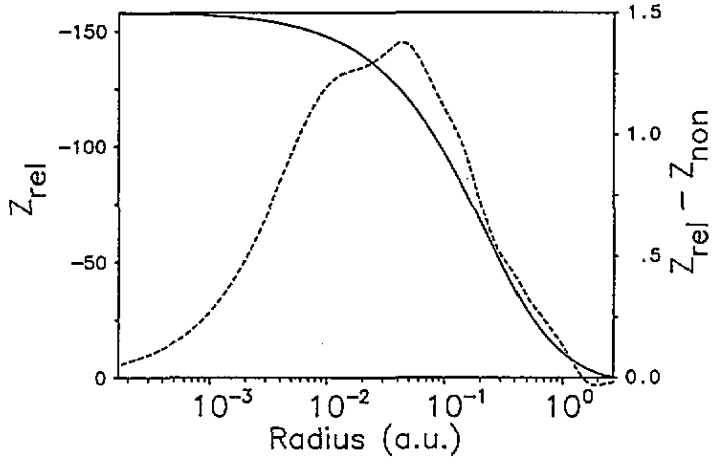

Figure 2. Effective charge Z_{rel} (——) and the difference $Z_{rel} - Z_{non}$ (– – –).

Recalling the effects of the relativistic corrections on the band structure, the levels with a large portion of s symmetry are raised by $\mathcal{H}_d$ but lowered even more by $\mathcal{H}_{mv}$.

Table 1. Relativistic orbital Compton profiles $J_{nlj}(q)$ in units of $\hbar/(mc^2)$.

q	1s + (2)	2s + (2)	2p − (2)	2p + (4)	3s + (2)	3p − (2)	3p + (4)
0.00	9.33E−03	3.32E−02	1.61E−02	1.82E−02	7.30E−02	4.27E−02	4.61E−02
0.05	9.33E−03	3.32E−02	1.61E−02	1.82E−02	7.30E−02	4.27E−02	4.61E−02
0.10	9.33E−03	3.32E−02	1.61E−02	1.82E−02	7.30E−02	4.27E−02	4.61E−02
0.15	9.33E−03	3.32E−02	1.61E−02	1.82E−02	7.29E−02	4.27E−02	4.61E−02
0.20	9.33E−03	3.32E−02	1.61E−02	1.82E−02	7.29E−02	4.27E−02	4.61E−02
0.30	9.33E−03	3.32E−02	1.61E−02	1.82E−02	7.28E−02	4.27E−02	4.61E−02
0.40	9.33E−03	3.32E−02	1.61E−02	1.82E−02	7.27E−02	4.27E−02	4.61E−02
0.50	9.33E−03	3.31E−02	1.61E−02	1.82E−02	7.25E−02	4.27E−02	4.61E−02
0.60	9.33E−03	3.31E−02	1.61E−02	1.82E−02	7.23E−02	4.27E−02	4.61E−02
0.70	9.33E−03	3.31E−02	1.61E−02	1.82E−02	7.21E−02	4.27E−02	4.61E−02
0.80	9.33E−03	3.31E−02	1.61E−02	1.82E−02	7.18E−02	4.27E−02	4.61E−02
1.00	9.33E−03	3.30E−02	1.61E−02	1.82E−02	7.11E−02	4.27E−02	4.61E−02
1.20	9.33E−03	3.30E−02	1.61E−02	1.82E−02	7.03E−02	4.27E−02	4.60E−02
1.40	9.32E−03	3.29E−02	1.61E−02	1.82E−02	6.94E−02	4.27E−02	4.60E−02
1.60	9.32E−03	3.28E−02	1.61E−02	1.82E−02	6.83E−02	4.27E−02	4.60E−02
1.80	9.32E−03	3.27E−02	1.61E−02	1.82E−02	6.71E−02	4.26E−02	4.60E−02
2.00	9.32E−03	3.26E−02	1.61E−02	1.82E−02	6.58E−02	4.26E−02	4.59E−02
2.40	9.31E−03	3.23E−02	1.61E−02	1.82E−02	6.29E−02	4.25E−02	4.58E−02
3.00	9.30E−03	3.18E−02	1.61E−02	1.82E−02	5.79E−02	4.22E−02	4.54E−02
4.00	9.27E−03	3.09E−02	1.61E−02	1.81E−02	4.85E−02	4.13E−02	4.41E−02
5.00	9.24E−03	2.96E−02	1.61E−02	1.81E−02	3.87E−02	3.96E−02	4.18E−02
6.00	9.20E−03	2.82E−02	1.61E−02	1.80E−02	2.96E−02	3.72E−02	3.86E−02
7.00	9.15E−03	2.66E−02	1.60E−02	1.79E−02	2.19E−02	3.40E−02	3.44E−02
8.00	9.09E−03	2.49E−02	1.59E−02	1.78E−02	1.58E−02	3.02E−02	2.98E−02
10.00	8.96E−03	2.12E−02	1.56E−02	1.74E−02	8.61E−03	2.20E−02	2.03E−02
15.00	8.53E−03	1.25E−02	1.43E−02	1.54E−02	5.56E−03	6.79E−03	5.27E−03
20.00	7.97E−03	6.28E−03	1.20E−02	1.23E−02	4.58E−03	2.09E−03	2.02E−03
30.00	6.64E−03	1.41E−03	7.03E−03	6.30E−03	1.06E−03	1.53E−03	1.69E−03
40.00	5.25E−03	8.17E−04	3.56E−03	2.77E−03	2.24E−04	1.02E−03	9.05E−04
60.00	3.00E−03	6.95E−04	8.60E−04	5.12E−04	1.65E−04	2.64E−04	1.70E−04
100.00	9.12E−04	2.14E−04	8.17E−05	3.04E−05	5.32E−05	2.35E−05	9.29E−06

$\mathcal{H}_{so}$ has no effect on these levels but lifts the degeneracy of the others, which are lowered slightly by $\mathcal{H}_d$ and $\mathcal{H}_{mv}$. The magnitude of the shifts differs by one order of magnitude between the highest atomic levels and the valence electrons.

As the effect of $\mathcal{H}_{mv}$ is dominant, the relativistic treatment enhances the binding of the core electrons to the nucleus. This is illustrated by the plot of the spherically averaged electron charge density in figure 1, obtained for the relativistic case (full curve), for the case $\alpha = 0$ (broken curve), and for the operator $-\Delta + V_{rel}$ (dotted curve). Comparing the full curve and the dotted curve shows that the operator $\Delta\mathcal{H}_{DS}$ causes the humps of the density to be enhanced and to be shifted towards the origin. Including $\Delta\mathcal{H}_V$ decreases this shift with increasing distance from the origin which can be seen by comparing the full curve and the broken curve. Obviously $\Delta\mathcal{H}_{DS}$ and $\Delta\mathcal{H}_V$ partially compensate each other. This compensation is maximal for the outermost core electrons. From figure 2 we learn that the nuclear Coulomb potential is more strongly screened in the relativistic treatment than in the non-relativistic case.

Table 1. (continued)

q	3d − (4)	3d + (6)	4s + (2)	4p − (2)	4p + (4)	4d − (4)	4d + (6)
0.00	2.97E−02	3.05E−02	1.50E−01	9.45E−02	1.02E−01	7.70E−02	7.88E−02
0.05	2.97E−02	3.05E−02	1.50E−01	9.45E−02	1.02E−01	7.70E−02	7.88E−02
0.10	2.97E−02	3.05E−02	1.50E−01	9.45E−02	1.02E−01	7.70E−02	7.88E−02
0.15	2.97E−02	3.05E−02	1.50E−01	9.45E−02	1.02E−01	7.70E−02	7.88E−02
0.20	2.97E−02	3.05E−02	1.49E−01	9.45E−02	1.02E−01	7.70E−02	7.88E−02
0.30	2.97E−02	3.05E−02	1.49E−01	9.45E−02	1.02E−01	7.70E−02	7.88E−02
0.40	2.97E−02	3.05E−02	1.47E−01	9.44E−02	1.02E−01	7.70E−02	7.88E−02
0.50	2.97E−02	3.05E−02	1.46E−01	9.44E−02	1.02E−01	7.70E−02	7.88E−02
0.60	2.97E−02	3.05E−02	1.44E−01	9.44E−02	1.02E−01	7.70E−02	7.88E−02
0.70	2.97E−02	3.05E−02	1.42E−01	9.44E−02	1.02E−01	7.70E−02	7.88E−02
0.80	2.97E−02	3.05E−02	1.39E−01	9.43E−02	1.02E−01	7.70E−02	7.88E−02
1.00	2.97E−02	3.05E−02	1.33E−01	9.41E−02	1.02E−01	7.69E−02	7.88E−02
1.20	2.97E−02	3.05E−02	1.26E−01	9.37E−02	1.01E−01	7.69E−02	7.88E−02
1.40	2.97E−02	3.05E−02	1.19E−01	9.31E−02	1.00E−01	7.69E−02	7.87E−02
1.60	2.97E−02	3.05E−02	1.11E−01	9.23E−02	9.91E−02	7.68E−02	7.86E−02
1.80	2.97E−02	3.05E−02	1.02E−01	9.12E−02	9.74E−02	7.66E−02	7.84E−02
2.00	2.97E−02	3.05E−02	9.35E−02	8.97E−02	9.54E−02	7.64E−02	7.81E−02
2.40	2.97E−02	3.05E−02	7.63E−02	8.56E−02	8.98E−02	7.54E−02	7.71E−02
3.00	2.97E−02	3.04E−02	5.34E−02	7.67E−02	7.82E−02	7.27E−02	7.39E−02
4.00	2.96E−02	3.04E−02	2.77E−02	5.70E−02	5.42E−02	6.35E−02	6.38E−02
5.00	2.95E−02	3.02E−02	1.70E−02	3.67E−02	3.21E−02	4.98E−02	4.92E−02
6.00	2.92E−02	2.99E−02	1.47E−02	2.12E−02	1.72E−02	3.53E−02	3.42E−02
7.00	2.87E−02	2.93E−02	1.46E−02	1.19E−02	9.73E−03	2.29E−02	2.17E−02
8.00	2.78E−02	2.84E−02	1.37E−02	7.63E−03	7.03E−03	1.39E−02	1.29E−02
10.00	2.53E−02	2.56E−02	8.84E−03	6.00E−03	6.48E−03	5.00E−03	4.61E−03
15.00	1.59E−02	1.56E−02	1.64E−03	3.69E−03	2.98E−03	2.47E−03	2.52E−03
20.00	7.95E−03	7.55E−03	1.37E−03	9.59E−04	6.81E−04	1.86E−03	1.80E−03
30.00	1.59E−03	1.41E−03	3.90E−04	3.46E−04	3.98E−04	4.53E−04	4.05E−04
40.00	3.27E−04	2.73E−04	6.69E−05	2.59E−04	2.34E−04	9.47E−05	7.90E−05
60.00	2.16E−05	1.59E−05	4.22E−05	6.94E−05	4.45E−05	6.13E−06	4.50E−06
100.00	4.43E−07	2.50E−07	1.39E−05	6.07E−06	2.39E−06	1.22E−07	6.89E−08

[27] have been used here. The absolute errors in the tabulated quantities depend on the orbital type and are estimated to be less than ±2.5 in the first omitted decimal place. This is the same accuracy as specified by Biggs. The presented CP values are very similar to those of Biggs but throughout are slightly larger at the origin and therefore smaller in the high-momentum region. Hence, the core-electron charge densities in the crystal are more delocalized than the atomic ones. This tendency is physically reasonable but the deviations from the atomic case are surprisingly small. The differences are $\leqslant 4$ in the third stated digit, which is the last significant one. Although one would expect the best agreement for the CPs of strongly bound electrons, the deviations are maximal for the 1s electron. From the close agreement with Biggs' results we may conclude that the many-body corrections beyond the one-particle scheme used here are small for the core electrons. This is not so with regard to the relativistic effect, as the above-mentioned partial compensation of $\Delta\mathcal{H}_{\mathrm{DS}}$ by $\Delta\mathcal{H}_V$ is small for the electrons in the vicinity of the nucleus.

The effects of $\mathcal{H}_{\mathrm{mv}}$ and $\mathcal{H}_{\mathrm{d}}$ on the CP of the 22 atom-like electrons (4f, 5s, 5p) are shown in figure 3(*a*). The eigenfunctions to $-\Delta + V_{\mathrm{rel}}$ yield the CP represented by the broken curve. The effects of the relativistic corrections on the momentum

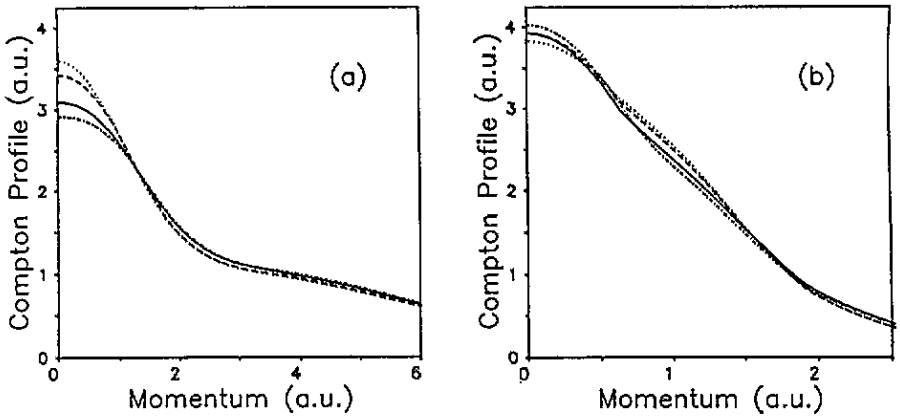

Figure 3. Effects of the operators $\mathcal{H}_d$ (· · · · ·), $\mathcal{H}_{mv}$ (— · —) and $\mathcal{H}_d + \mathcal{H}_{mv} + \mathcal{H}_{so}$ (——) on the Compton profile, calculated with the eigenfunctions of $-\Delta + V_{rel}$ (– – –). (*a*) CP of the 4f, 5s and 5p electrons. (*b*) CP of the valence electrons.

density and charge density are complementary to each other. $\mathcal{H}_{mv}$ binds the electrons more strongly to the nucleus and therefore the CP is broadened (chain curve). On the other hand, the influence of $\mathcal{H}_d$ is smaller and has opposite sign: the CP is enhanced near the origin and lowered in the upper momentum region (dotted curve). All three relativistic corrections together yield the full curve. Here the spin–orbit coupling contributes to the CP by approximately 0.1%. This is the same order of magnitude as the integration error of the spherical averaging process. For completeness, figure 3(*b*) shows the CPs of the 11 valence electrons. Owing to the better screening of the Coulomb potential in the relativistic case the d and f electrons are less localized. This behaviour is visible from figures 4(*a*)–(*c*), showing the effect of $\Delta\mathcal{H} = \mathcal{H}_{rel} - \mathcal{H}_{non}$ on the 46 innermost core electrons (*a*), the 22 outermost core electrons (*b*), the 11 valence electrons (*c*) and all electrons (*d*). In the case of the 11 valence electrons, the effect of $\Delta\mathcal{H}$ is changed in sign, i.e. $\mathcal{Z}_{rel}$ leads to an expansion of the d and f valence electrons. The dip at $p \simeq 0.65$ au is caused by the discontinuous occupation of the electron states at the Fermi energy. In figure 4(*d*) the total profiles for zero momentum differ by 1.7% only.

6. Conclusions

On the basis of relativistic self-consistent MAPW calculations, the effects of mass–velocity, the Darwin term and spin–orbit coupling on the spherically averaged Compton profile of gold have been discussed.

Comparisons with the results of non-relativistic calculations show the importance of Darwin and mass–velocity corrections. Their effects on the CPs are easily understood on the basis of the well known behaviour of the electron charge density in real space, as real and momentum space are complementary to each other. The spin–orbit coupling contributes only an amount of 0.1% and is therefore negligible.

The orbital CPs agree very well with the results of relativistic Hartree–Fock calculations by Biggs *et al.* From this fact it may be concluded that the local-density approximation for the exchange potential is well suited even for the highly inhomogeneous electron gas in gold.

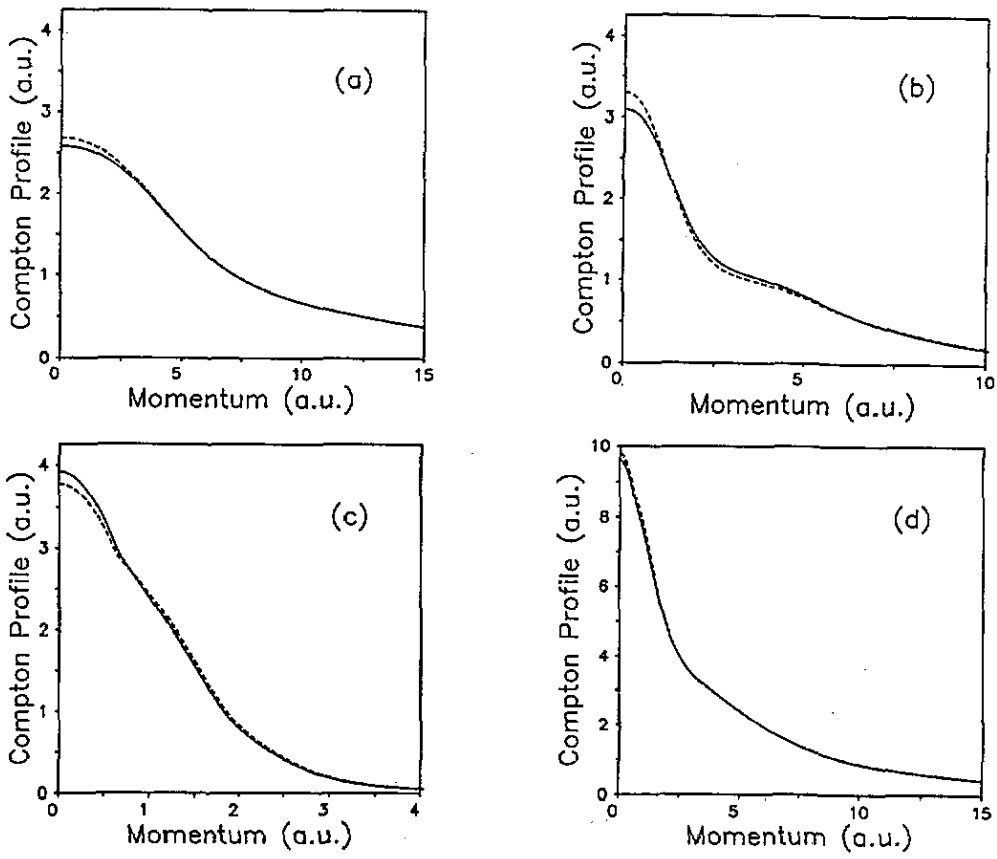

Figure 4. Relativistically (——) and non-relativistically (– – –) determined Compton profiles of (*a*) the 46 innermost electrons, (*b*) the 22 atom-like electrons (4f, 5s, 5p electrons), (*c*) the 11 valence electrons, (*d*) all 79 electrons.

Experimental studies of the CP of gold are desirable in order to check the validity of the present calculations and the models used.

Acknowledgments

There have been many helpful discussions with Dr H Stöhr on the MAPW method. His friendly support in numerical questions is gratefully acknowledged. Thanks are also due to Dipl Phys B Sporkmann for results from an interpolation of the presented band structure. The authors would like to thank Professor F Bell for stimulating discussions. All calculations were performed on the CDC Cyber 995 computer of the Leibniz Rechenzentrum in Munich.

Appendix

An analytical expression for the CP of the 1s electron in the Coulomb potential $-2Z/r$ for the momentum transfer $q = 0$ can be obtained straightforwardly by

applying equations (1) and (4) to the solution of the Dirac equation:

$$g_{1s}(r) = -N(1+\rho)^{1/2}e^{-Zr} \qquad f_{1s}(r) = +N(1-\rho)^{1/2}e^{-Zr}/\alpha$$

where

$$\rho = (1-\alpha^2Z^2)^{1/2} \qquad N = \frac{(2Z)^{\rho+1/2}}{[2\Gamma(2\rho+1)]^{1/2}}.$$

The method of calculation will be outlined by the example of the second integral of equation (4), which contains the small component $f(r)$. Apart from normalization factors, we have to calculate

$$\mathcal{J} := \int_{q=0}^{\infty} dp\, p\left(\int_0^{\infty} dr\, r^{\rho+1}\mathcal{J}_1(pr)e^{-Zr}\right)^2$$
$$= 2\int_0^{\infty} dr \int_0^{r} dr'\, r^{\rho+1}r'^{\rho+1}e^{-Zr}e^{-Zr'}I(r,r') \tag{A1}$$

where

$$I(r,r') = \int_0^{\infty} dp\, p\mathcal{J}_1(pr)\mathcal{J}_1(pr').$$

The spherical Bessel function $\mathcal{J}_1$ can be expressed by the cylindrical one $J_{3/2}$. After substitution the resulting integral can be found in [46], vol II, p 48, equation (6):

$$I(r,r') = \tfrac{2}{3}r^{-3}r'F(2,1/2;5/2;(r'/r)^2) \qquad \text{for } r' < r. \tag{A2}$$

In equation (A2) F denotes the hypergeometric function. Setting $r'/r = x$ in (A1) and replacing $I(r,r')$ by (A2) the r integration can be carried out yielding the one-dimensional integral:

$$\mathcal{J} = \frac{4\Gamma(2\rho+2)}{3Z^{2\rho+2}}\int_0^1 dx\, \frac{x^{\rho+2}}{(1+x)^{2\rho+2}}F(2,1/2;5/2;x^2). \tag{A3}$$

With the aid of Gauss' relations for contiguous functions ((15.2.10) and (15.2.12) in [47]) and the special elementary cases of the Gauss series ((15.1.4) and (15.1.9) in [47]) the hypergeometric function can be written as follows:

$$F(2,1/2;5/2;x^2) = -\frac{3}{4x^2} + \frac{31+x^2}{8x^3}\ln\left(\frac{1+x}{1-x}\right). \tag{A4}$$

From the two terms on the right-hand side of equation (A4) two integrals remain to be solved. For the first one

$$\int_0^1 dx\, \frac{x^{\rho}}{(1+x)^{2\rho+2}} = \frac{1}{\rho+1}F(2\rho+2,\rho+1;\rho+2;-1) = \frac{1}{\rho+1}\frac{\pi^{1/2}}{2^{2\rho+2}}\frac{\Gamma(\rho+2)}{\Gamma(\rho+3/2)}$$

see [48], p 284, equation (3.194) and [47], p 557, equation (15.1.21). The second

$$\int_0^1 \mathrm{d}x\, \frac{x^{\rho-1}+x^{\rho+1}}{(1+x)^{2\rho+2}} \ln\left(\frac{1+x}{1-x}\right) = -2^{-2\rho}\int_0^1 \mathrm{d}y\,(1-y^2)^{\rho-1}(1+y^2)\ln y$$
$$= -2^{-(2\rho+2)}\{B(1/2,\rho)[\psi(1/2)-\psi(1/2+\rho)]$$
$$+ B(3/2,\rho)[\psi(3/2)-\psi(3/2+\rho)]\}$$

can be found in [48], p 538, equation (4.253). In the last expression B designates the beta function, which can be expressed by gamma functions. Summing over all terms, the contribution of the small component becomes

$$J_{1s}^{(f)}(0) = \frac{(1-\rho)(2\rho+1)}{8\pi^{1/2}}\frac{1}{Z}\frac{\Gamma(\rho+1)}{\Gamma(\rho+3/2)}$$
$$\times\left(-2+\frac{1}{2\rho}[(2\rho+2)(\psi(\rho+3/2)-\psi(1/2))-4]\right).$$

A similar calculation for the contribution of the large component yields the result:

$$J_{1s}^{(g)}(0) = \frac{(1+\rho)(2\rho+1)}{8\pi^{1/2}}\frac{1}{Z}\frac{\Gamma(\rho+1)}{\Gamma(\rho+3/2)}[\psi(\rho+3/2)-\psi(1/2)].$$

Finally, equation (6) is given by the sum:

$$J_{1s}^{c}(0) = J_{1s}^{(g)}(0) + J_{1s}^{(f)}(0).$$

References

[1] Hohenberg P and Kohn W 1964 *Phys. Rev.* **136** B864
[2] Moruzzi V L, Janak J F and Williams A R 1978 *Calculated Electronic Properties of Metals* (New York: Pergamon)
[3] Kohn W and Sham L J 1965 *Phys. Rev.* **140** A1133
[4] Rajagopal A K and Callaway J 1973 *Phys. Rev.* B **7** 1912
[5] Rajagopal A K 1978 *J. Phys. C: Solid State Phys.* **11** L943
[6] Gunnarsson O and Lundqvist B I 1976 *Phys. Rev.* B **13** 4274
[7] MacDonald A H and Vosko S H 1979 *J. Phys. C: Solid State Phys.* **12** 2977
[8] Henderson G A 1981 *Phys. Rev.* A **23** 19
[9] Englert B G 1992 *Phys. Rev.* A **45** 127
[10] Ribberfors R 1975 *Phys. Rev.* B **12** 2067
[11] Eisenberger P and Platzman P M 1970 *Phys. Rev.* A **2** 415
[12] Holm P 1988 *Phys. Rev.* A **37** 3706
[13] Perkkiō S *et al* 1991 *Phys. Status Solidi* b **168** 657
[14] Mohammad F M *et al* 1989 *Phys. Status Solidi* b **152** 145
[15] Mittal U, Sharma B K, Mohammad F M and Ahuja B L 1988 *Phys. Rev.* B **38** 12208
[16] Sharma B K *et al* 1988 *Phys. Rev.* B **37** 6821
[17] Sharma B K *et al* 1987 *Phys. Status Solidi* b **141** 177
[18] Tomak M *et al* 1985 *Phys. Status Solidi* b **127** 221
[19] Manninen S and Paakkari T 1981 *Phil. Mag.* **44** 127
[20] Williams B G (ed) 1977 *Compton Scattering* (New York: McGraw-Hill) p 159
[21] Berggren K F 1972 *Phys. Rev.* B **6** 2156
[22] Bauer G E W and Schneider J R 1983 *Z. Phys.* B **54** 17

[23] Bauer G E W and Schneider J R 1985 *Phys. Rev.* B **31** 681
[24] Papanicolaou N I, Bacalis N C and Papaconstantopoulos D A 1986 *Phys. Status Solidi* b **137** 597
[25] Koelling D D and Harmon B N 1977 *J. Phys. C: Solid State Phys.* **10** 3107
[26] Spies R and Bell F 1988 *Z. Phys.* B **70** 163
[27] Biggs F, Mendelsohn L B and Mann J B 1975 *At. Data Nucl. Data Tables* **16** 201
[28] Koelling D D 1981 *Rep. Prog. Phys.* **44** 139–212 and references therein
[29] Foldy L L and Wouthuysen S A 1950 *Phys. Rev.* **78** 29
[30] Cowan R D and Griffin D C 1976 *J. Opt. Soc. Am.* **66** 1010
[31] Conklin J B Jr, Johnson L E and Pratt G W Jr 1965 *Phys. Rev.* **137** A1282
[32] Marcus P M 1967 *Int. J. Quantum Chem.* **1** 576
[33] Bross H 1964 *Phys. Kondens. Mater.* **3** 119
[34] Bross H 1968 *Helv. Phys. Acta* **41** 717
[35] Bross H 1968 *Z. Phys.* **215** 485
[36] Bross H *et al* 1970 *Phys. Rev.* B **2** 3098
[37] Bross H *et al* 1971 *Computational Methods in Band Theory* (New York: Plenum)
[38] Hofmann I and Bross H 1969 *Z. Phys.* **229** 123
[39] Schiekel F B 1984 *Thesis* University of Munich
[40] Reinisch H 1990 *Thesis* University of Munich
[41] Bross H and Eder R 1987 *Phys. Status Solidi* b **144** 175
[42] Williams E R and Olsen P T 1979 *Phys. Rev. Lett.* **42** 1575
[43] Bross H 1982 *J. Phys. F: Met. Phys.* **12** 2249
[44] Christensen N E and Seraphin B O 1971 *Phys. Rev.* B **4** 3321
[45] Bross H 1978 *J. Phys. F: Met. Phys.* **8** 2631
[46] Erdélyi A (ed) 1954 *Tables of Integral Transforms* (New York: McGraw-Hill)
[47] Abramowitz M and Stegun I (ed) 1960 *Handbook of Mathematical Functions* (New York: Dover)
[48] Gradshteyn I S and Ryzhik I M 1965 *Tables of Integrals, Series and Products* (New York: Academic)